β-actin mRNA interactome mapping by proximity biotinylation

Joyita Mukherjee[1], Orit Hermesh[1], Nicolas Nalpas[2], Mirita Franz-Wachtel[2], Boris Maček[2], Ralf-Peter Jansen[1,3]

1 Interfaculty Institute of Biochemistry, University of Tübingen, Tübingen, Germany.

2 Proteome Center Tübingen, University of Tübingen, Tübingen, Germany.

3 Corresponding author:
Ralf-Peter Jansen
University of Tübingen
Interfaculty Institute of Biochemistry
Hoppe-Seyler-Strasse 4
72076 Tübingen, Germany
Phone: +49-7071-2974161
Email: ralf.jansen@uni-tuebingen.de

KEYWORDS:

RNA-BioID, mRNA localization, FUBP3, RNA binding protein, protein−RNA interaction, object-based co-localization, Label free quantification.

RUNNING TITLE:

RNA-BioID identifies β-actin mRNA-associated proteins

ABSTRACT

The molecular function and fate of mRNAs are controlled by RNA binding proteins (RBPs). However, identification of the interacting proteome of a specific mRNA in vivo is still very challenging. Based on the widely-used RNA tagging with MS2 aptamers for RNA visualization, we developed a novel RNA proximity biotinylation (RNA-BioID) method by tethering biotin ligase (BirA*) via MS2 coat protein (MCP) at the 3'UTR of endogenously MS2 tagged β-actin mRNA in mouse embryonic fibroblasts (MEFs). We demonstrate the dynamics of the β-actin mRNA interactome by characterizing its changes upon serum-induced localization of the mRNA. Apart from the previously known interactors, we identified over 60 additional β-actin associated RBPs by RNA-BioID, among them the KH-domain containing protein FUBP3/MARTA2 has shown to be required for β-actin mRNA localization. This protein binds to the 3'-untranslated region of β-actin mRNA, is essential for β-actin mRNA localization but does not interact with the characterized β-actin zipcode element. RNA-BioID provides a tool to identify new mRNA interactors and to study the dynamic view of the interacting proteome of endogenous mRNAs in space and time.

INTRODUCTION

The spatial distribution of mRNAs contributes to the compartmentalized organization of the cell and is required for maintaining cellular asymmetry, proper embryonic development and neuronal function (1). Localized mRNAs contain cis-acting sequences, termed zipcodes or localization elements that constitute binding sites for RNA-binding proteins (RBPs) (1). Together with these RBPs, localized mRNAs form transport complexes containing molecular motors such as kinesin, dynein, or myosin (2, 3). These ribonucleoprotein complexes (RNPs) usually include accessory factors such as helicases, translational repressors, RNA stability factors or ribosomal proteins (3). Thus, mRNPs as functional units do not only contain the information for an encoded polypeptide but also determine the precise spatio-temporal regulation of its translation, thereby facilitating the correct subcellular localization of the translation product (4).

One of the best-studied localized mRNAs is β-actin that encodes the β isoform of the cytoskeleton protein actin (5, 6). β-actin mRNA is localized to the protrusion of migrating fibroblasts (7) where its local translation critically contributes to the migrating behaviour of this cell type (8–11). In developing mouse (12) and *Xenopus* (13) neurons, β-actin mRNA is transported to the growth cone during axonal

extension and its deposition and local translation is highly regulated by external cues. In addition, translation of this mRNA in dendritic spines is involved in re-shaping the postsynaptic site of synapses (14). A well-defined localization element is in the proximal region of the β-actin 3' untranslated region (3'-UTR) (15). This cis-acting signal is recognized by the zipcode-binding protein ZBP1 (16), an RBP of the conserved VICKZ RNA-binding protein family (17). ZBP1 (also called IGF2BP1 or IMP1) interacts with the zipcode via two K-homology (KH) RNA-binding domains (10) and is required for RNA localization in fibroblasts and neuron (18). In addition, it controls translation of β-actin by blocking the assembly of ribosomes at the start codon (19). IGF2BP1 appears to act as key RBP in β-actin mRNA distribution but several other proteins have been involved in β-actin mRNA localization, although their molecular function is less clear. Other proteins like IGF2BP2 (20), RACK1 (21), KHSRP/FUBP2 (22), KHDBRS1/SAM68 (23, 24), and FMR1 (25), HuR (26) has also shown to be influencing in β-actin mRNA localization.

To fully understand mRNA localization and its regulation, it is important to know the proteins, those are binding and controlling these mRNAs. Major technological advances like CLIP (crosslinking and immunoprecipitation) combined with next-generation sequencing allow the identification of RNAs bound to specific RBPs (27) or the system-wide identification of RBPs that bind to polyA RNA (28, 29). However, the major approaches to determine which proteins associate with a specific RNA are affinity purification of modified or tagged RNAs together with their bound proteins, or co-immunoprecipitation of RNP components with the help of known RNA-specific RBPs. In addition, affinity capturing of specific RNPs with hybridizing antisense probes or via integrated aptamers has been successfully used (30–33). A serious limitation of these techniques is the potential loss of low affinity binders during purification, which has so far been addressed by *in vivo* UV cross-linking prior to cell lysis. However, cross-linking enhances only the recovery of RBPs directly contacting nucleobases and therefore does not overcome the loss of other physiologically important RNA interactors, e.g. motor or adapter proteins. These limitations could be overcome by *in vivo* labelling of proteins while they are associated with the target RNA. BioID (34) has been successfully used to detect subunits of large or dynamic protein complexes like the nuclear pore complex (35) or centrosome (36). In BioID, a protein of interest is fused to a mutant version of the *E. coli* biotin ligase BirA (BirA*) that generates AMP-biotin ('activated biotin'), which reacts with accessible lysine residues in its vicinity (37). After lysis, biotinylated proteins can be isolated via streptavidin affinity purification and identified using standard mass spectrometry techniques. Recently,

BioID has also been applied to identify proteins associated with the genomic RNA of ZIKA virus (38). In this study, we have used BioID to characterize the proteome of an endogenous, localized β-actin mRNP. We report here that tethering of BirA* to an endogenous transcript does not only allow the identification of its associated proteins but can also be used to probe the environment of this mRNA. This approach allows, with high confidence, to identify novel functional β-actin interactors that are as highly enriched as the reported β-actin RBPs. This is exemplified by FUBP3/MARTA2, an RBP from the conserved FUBP family of proteins (39, 40), which was previously shown to mediate dendritic targeting of MAP2 mRNA in neurons (41, 42) but is shown here to bind to and facilitate localization of β-actin mRNA to fibroblast protrusions. FUBP3 does not bind to the zipcode or IGF2BP1 but mediates β-actin RNA localization by binding to another site in its 3'-UTR.

RESULTS

Tethering biotin ligases to the 3'-UTR of β-actin mRNA

In order to tether BirA* to the 3'-UTR of β-actin mRNA (Fig. 1*A*), we stably expressed a fusion of the nuclear localized signal (NLS) MS2 coat protein (MCP) (43), GFP and BirA* (MCP-GFP-BirA*) in immortalized mouse embryonic fibroblasts (MEFs) from transgenic β-actin-24 MBS mice (Fig. 1*A*, lower panel) (9). These mice have both β-actin gene copies replaced by β-actin with 24 MS2 binding sites (MBS) in their distal 3'-UTR. In parallel, NLS-MCP-GFP-BirA* was stably expressed in WT (wildtype) MEFs with untagged β-actin mRNA, to generate a control cell line to eliminate background biotinylation due to the presence of constitutive expression of BirA* (Fig. 1*A*, upper panel). Both the constructs contain 2 copies of the MCP protein so finally, a maximum of 12 GFP and 12 BirA* can binds on the mRNA at a time. Since biotinylation or the expression of the MCP-GFP-BirA* might affect localization of the β-actin mRNA, we checked for the proper targeting of β-actin mRNA to cell protrusions by smFISH, using probes against the β-actin ORF. To induce β-actin mRNA localization, WT (unmodified) MEFs and β-actin MBS/GFP-BirA* MEFs were serum starved for 24 hrs followed by stimulation with serum addition for 2 hrs. In both MEF lines, we observed the typical targeting of the β-actin mRNA to the cell protrusions (Fig. 1*B*, arrows). Furthermore, we ensured that cells with similar expression level of MCP-GFP-BirA* constructs were sorted by FACS (fluorescence activated cell sorting)(Data not shown) against GFP laser and we also checked that the expression of MCP-GFP-BirA* does not alter β-actin mRNA and protein levels (Fig.1*C, D*).

As shown before (37), we found no difference in the biotinylation labelling efficiency in presence of 50 µM-300µM of biotin for 6-48 hrs. (Data not shown). To get the maximum biotinylated proteins, proximity labelling was performed by addition of 50 µM biotin to the medium for 24 hrs. To test if proximity labelling can identify known β-actin mRNA-associated proteins, we affinity purified biotinylated proteins followed by western blot detection of IGF2BP1 (mouse ZBP1). IGF2BP1 was biotinylated in MEFs expressing β-actin-MBS/GFP-BirA* but not in those expressing only GFP-BirA* (Fig. 1*E*), which demonstrates that our tool can successfully biotinylate zipcode-interacting proteins. To differentiate between endogenously biotinylated proteins to RNA mediated biotinylated proteins, we did streptavidin pulldown in cells expressing β-actin-MBS / GFP-BirA* and in cells expressing only MCP-GFP, we observed biotinylation of numerous proteins in addition to endogenous biotinylated proteins (Fig. S1). We expected that a major fraction of biotinylated proteins is MCP-GFP-BirA* itself. We therefore aimed at depleting the fusion protein from the lysate by GFP pulldown prior to streptavidin affinity purification. To our surprise, most of the biotinylated proteins were enriched in the GFP pulldown fraction (Fig.S1), which is likely due to co-purification of MCP-GFP-BirA*, β-actin mRNA and biotinylated proteins binding to the mRNA or the fusion protein. RNA degradation with RNase A (Fig.S2) shifted a large part of the biotinylated proteins into the streptavidin fraction (Fig.S1), supporting the idea that most of the biotinylated proteins are associated with β-actin mRNA. Additional treatment with high salt and 0.5% SDS further optimized the streptavidin affinity purification and decreased the background binding of the magnetic beads used in this purification (Fig.S1).

β-actin mRNA interactors under serum-induced and uninduced conditions

β-actin mRNA localization to the lamellipodia of chicken and mouse fibroblasts increases after serum induction (44). It was also shown that during serum starvation, cells enter a quiescent phase of the cell cycle (45) with an overall reduction in actin stress fibres or focal adhesions (44). As shown before (5), chicken and mouse fibroblasts induce β-actin mRNA localization after serum addition (Fig.S3) and the fraction of MEFs with β-actin localized to lamellipodia increases within one hour but remains constant over the next hours (Data not shown).

To determine and compare the β-actin associated proteomes in uninduced and serum-induced MEFs, we performed RNA-BioID under both conditions (three replicate experiments each). Unspecific as well as endogenous biotinylation was assessed by performing BioID in MEFs expressing MCP-GFP-BirA*

in the absence of MS2 aptamers in β-actin mRNA. Affinity-captured biotinylated proteins were identified and quantified by mass spectrometry using label free quantification (LFQ; see Methods). Principal component analysis of the datasets revealed that the different conditions cluster apart from each other in dimensions 1 and 2 (explaining 33.8% and 15.5% of variance), while the replicates with the same conditions cluster together demonstrating biological reproducibility (Fig.S4). Calculating the Spearman correlation between all sample types and replicates (Fig.S5) supports the high reproducibility between biological replicates (correlation ≥ 0.97). In addition, it showed better correlation between uninduced and induced samples (average 0.95) compared to control. In total, we found 169 (or 156) significantly enriched proteins in induced (or uninduced) MEFs compared to control cells (Fig.S6). Of these, 47 were enriched only under induced conditions (Supplementary excel sheet). To assess the differential enrichment of the proteins under each condition, a Tukey post-hoc test was performed after the ANOVA, and the significance was set to an adjusted p-value of 0.05 following Benjamini-Hochberg multiple correction testing (see Materials and Methods). A large fraction of the enriched proteins (30% and 34%) under induced or uninduced conditions over control represent RNA-binding proteins (Fig.2, red solid circles). Among these are RBPs (IGF2BP1, IGF2BP2, KHSRP, KHDRBS1, FMR1, HuR, RACK1, named in red) already known to control specific aspects of β-actin mRNA physiology. Other enriched RBPs have been associated with the localization of mRNAs in other cell types or organisms, including STAU1 and STAU2 (46, 47), SYNCRIP (48), and FUBP3 (49). Furthermore, 85 proteins were significantly enriched under serum-induced compared to uninduced conditions (S5). However, the majority of the above-mentioned RBPs (including IGF2BP1) become biotinylated under induced as well as uninduced conditions, indicating that they are associated with β-actin mRNA under both conditions (Fig.2*C*).

A cluster analysis (Fig.3) reveals at least five different patterns of biotinylated proteins in induced, non-induced and control MEFs (Fig.3*B, C*). In control MEFs, we see enrichment of mainly nuclear proteins (cluster 1). This is expected since the unbound MCP-GFP-BirA* is enriched in the nucleus due to an N terminal nuclear localization sequence (9). Cluster 1 also contains abundant cytoplasmic proteins like glycerol aldehyde phosphate dehydrogenase (GAPDH). Cluster 3 represents proteins that are equally found in MEFs under all conditions and contains e.g. ribosomal proteins. Proteins allocated to the other three clusters (clusters 2, 4, 5) are overrepresented in the biotinylated proteome of MEFs expressing β-actin-MBS/GFP-BirA*. Of specific interest are clusters 4 and 5. In cluster 4, with proteins that are

more biotinylated under serum-induced conditions, we find RNA-binding proteins, among them FMR1 and KHSRP that have been reported to function in β-actin mRNA localization or bind to IGF2BP1. Another group of proteins that are enriched in this cluster are proteins of the actin cytoskeleton (e.g. Filamin B, Cofilin-1, Myh9, Tpm4, Plastin-3). Their enrichment likely reflects the deposition of the β-actin mRNA in the actin-rich cortical environment of the MEF's protrusions. Finally, cluster 5 contains proteins found in β-actin-MBS MEFs under induced as well as non-induced conditions but not in control MEFs. This cluster shows an enrichment for proteins involved in mRNA-binding, RNP constituents or ribosomal proteins. Since this cluster contains the zipcode-binding protein IGF2BP1, we hypothesized that other proteins in this cluster, e.g. FUBP3 are likely candidates for β-actin mRNA regulatory factors.

FUBP3 is a component of the β-actin mRNP

To confirm the association of FUBP3 and MS2-tagged β-actin mRNA, we combined single molecule FISH (smFISH) with immunofluorescence (smFISH-IF) using probes against the MBS part and antibody against FUBP3 (Fig.4*A*). An object based colocalization analysis of snapshot images was used to determine the extent of colocalization with β-actin mRNA (50). To ensure that colocalization of signals from the smFISH with those from the IF did not occur by chance, we included a positive and negative controls for RNA binding proteins that bind (IGF2BP1) or do not bind (VIGILIN) β-actin mRNA (Fig.S8). Additionally, we also performed smFISH with differently coloured probes against the β-actin ORF and the MBS part which allowed us to estimate the feasibility of our method to detect colocalization. The distances of particles detected with β-actin ORF probes from particles detected with MBS were determined and their distribution is shown in Fig.S9. As the distances between the two smFISH probes were mostly distributed under 250 nm, which is consistent with the proposed size of RNA granules in neurons (100-250 nm) (51) we defined spots whose centers were less than 250 nm apart as colocalizing. At this distance, 70% of β-actin ORF probes were found to colocalize with MS2 probes which is slightly less than seen in previous reports (ranging between 73%-90%) (51, 52) indicating that our method might rather underestimate the extent of colocalization. Nevertheless, we found that 32% of MBS spots colocalized with FUBP3, which is similar to IGF2BP1(36%) but different from VIGILIN (21% colocalization) (Fig.4*B*).

FUBP3 and IGF2BP1 binds on different regions of β-actin mRNA and interacts with each other in an RNA dependent manner

To validate our colocalization experiments, we performed co-immunoprecipitation of β-actin mRNA with FUBP3 and IGF2BP1 (Fig.5*A*). Both proteins co-precipitate four tested mRNAs (β-actin, Cofilin1, Igf2bp1, Fubp3). In case of IGF2BP1, it binds to all the mRNAs tested, which reflects previous observations in Hela cells, where almost 3% of the transcriptome was shown to bind to IGF2BP1 (53). β-actin binding to FUBP3 (nearly 23% of input bound to FUBP3) was quite similar to IGF2BP1 (nearly 37%), which correlates with the colocalization analysis (Fig.4). In contrast, FUBP3 and IGF2BP1 binds another localized mRNA, Cof1 (54) to a similar extent (48%). As a negative control we have chosen the 14KH domain containing protein Vigilin, which we also found to be non-significant in the RNA-BioID mass spec data. Since co-precipitation of these mRNAs with FUBP3 could be indirect, e.g. via IGF2BP1, we used recombinant glutathione S transferase (GST)-FUBP3 and IGF2BP1 (Fig.S10) in pulldown assays to test direct binding to *in vitro* transcribed RNA fragments of β-actin mRNA. We selected the 54-nucleotide localization zipcode element of β-actin, a 49-nucleotide long region after the zipcode (proximal zipcode; (15)) and the 643bp long whole β-actin 3'-UTR. RNA capturing by GST fusion proteins was performed from *E. coli* lysates, which allows bacterial RBPs to serve as endogenous competitors for RNA binding. RNA captured by the GST fusion proteins was detected by quantitative RT-PCR and normalized to the input. Lysates expressing only GST protein and a zipcode mutant RNA unable to bind to IGF2BP1 (55, 56) served as negative controls. Unlike IGF2BP1, FUBP3 does not bind to the zipcode but does interact with the 3'UTR of β-actin mRNA, suggesting that it recognizes a different site in the 3'-UTR (Fig.5*B*). A recent publication (57) revealed that FUBP3 binds the motif UAUA, which is also present at the 3'UTR of β-actin mRNA, 459bp downstream of the stop codon. To further substantiate our finding that FUBP3 can bind independently of IGF2BP1 to β-actin mRNA, we performed co-immunoprecipitation experiments of IGF2BP1 and FUBP3 (Fig.5*C*) in presence or absence of RNase A. We did not detect co-immunoprecipitation of IGF2BP1 and FUBP3 when the lysates were treated with RNase. However, we see that IGF2BP1 co-purifies with FUBP3, indicating RNA dependent interaction between these two proteins. We conclude that FUBP3 does not bind to β-actin mRNA via IGF2BP1 rather they bind on the same mRNA but on different sites.

To identify the KH domain(s) of FUBP3 responsible for binding β-actin mRNA, we introduced mutations in the conserved KH domains of the protein. Each functionally important G-X-X-G motif in the four KH

domains was changed to the inactive G-D-D-G (58) and individual mutant proteins were transiently expressed in MEFs as C-terminally tagged mCherry fusion protein. The G-D-D-G mutation in KH domain 2 resulted in loss of the cytoplasmic punctate signal seen in wild type FUBP3, which is reminiscent of punctate pattern observed for mRNPs (Fig.5*D*). We conclude that KH2 in FUBP3 is important for its integration into RNP particles and likely constitutes the critical domain for RNA binding.

Loss of FUBP3 affects β-actin mRNA localization

To validate that proteins identified by RNA-BioID are functionally significant for the mRNA used as bait, we performed knockdown experiments for Fubp3. Knockdown of Igf2bp1 was used as a positive control for a factor involved in β-actin localization. The effectiveness of the knockdown was validated by checking mRNA levels by RT-PCR and protein levels by western blot against IGF2BP1 and FUBP3, using GAPDH as a loading control as it remains unaffected in the RNA BioID (Fig.6*A*, *B*, Fig.3*C* and Fig.S11,). The effect of the knockdown on β-actin mRNA localization was assessed by smFISH (Fig.6*C* and Fig.S12). In control cells, up to 47% of MEFs show localized β-actin mRNA in their protrusions (Fig.6*C*). IGF2BP1 knockdown reduces this to 32% while FUBP3 knockdown leads to a reduction to 21% (Fig.6*C*). This indicates that FUBP3 is important for β-actin mRNA localization. In addition, we found that knockdown of Igf2bp1 or Fubp3 only mildly changes β-actin mRNA levels (79% of wild type in case of Igf2bp1 knockdown, 93% in case of Fubp3). In contrast, the level of β-actin protein increases to 120%, or 150%, respectively (Fig.6*A*, *B*). In case of IGF2BP1, this is consistent with previous reports showing that the protein acts as translational repressor of β-actin mRNA and that localization defects seen after loss of IGF2BP1 are due to premature translation of the mRNA before reaching its normal destination site (19, 59). FUBP3 could perform a similar role on β-actin mRNA.

DISCUSSION

Proximity biotinylation has facilitated the characterization of dynamic protein complexes by *in vivo* labelling of interaction partners. Here, we exploit this approach and demonstrate its utility for identifying functionally relevant RNA-binding proteins of a specific mRNA, mammalian β-actin. This is achieved by combining MS2 tagging of the mRNA of choice and co-expression of a fusion protein of the MS2 coat protein (MCP) and the biotin ligase (BirA*).

The primary goal for an RNA-based BioID is the identification of novel RNA interactors. As seen before in several proximity labelling (BioID or APEX-driven) approaches (37, 60, 61), the number of identified potential interactors for β-actin is far higher than the number of proteins identified in classical co-immunoprecipitation or co-affinity purification approaches. This might be due to the higher sensitivity of proximity labelling or its propensity to allow capturing of transient interactors (34). Although this can result in a skewed view of the actual components of a complex due to the rapid change in the composition of mRNP, it is beneficial to identify all the mRNP components during the life stages of an mRNA. The most highly represented class of proteins were RBPs (Fig.3 and Fig.S7*B*), among them all RBPs that have been previously associated with localization, translational control or (de)stabilization of β-actin mRNA. Other RBPs like survival of motor neuron 1 (SMN1), which supports the association of IGF2BP1 with β-actin mRNA (62, 63), were also found to be enriched in MEFs expressing β-actin-MBS compared to control MEFs, although with lower significance (p-value < 0.1).

We also analysed our dataset for motor proteins involved in mRNA transport. Neither MYH10 (64) nor KIF11 (65) that have been suggested to work as β-actin mRNA transport motors were found as biotinylated proteins. The only motor we identified is MYH9, the heavy chain of a MYH10 related class II-A myosin although it was not significantly enriched (p = 0.08). The lack of motor proteins is compatible with a recent observation that β-actin localization in fibroblasts works primarily by diffusion to and trapping in the microfilament-rich cortex (66). This is also corroborated by our finding that components of the actin-rich cell protrusion (Fig:3, cluster 4) are heavily biotinylated in MEFs after serum-induced localization of β-actin.

Overall, the cluster analysis shows that the majority of previously identified β-actin RBPs behave similarly under the two tested conditions (serum-induced and uninduced MEFs). This not only indicates that they interact with β-actin mRNA in MEFs even under steady state conditions, but It also makes it likely that other proteins, especially RBPs, found in this cluster might represent so far unknown β-actin mRNA interactors. By choosing the far-upstream binding protein FUBP3 as a potential candidate we demonstrate that this assumption holds true for at least this protein. FUBP3 not only binds to β-actin mRNA but its knockdown also results in a similar decrease of β-actin localization to the protrusions as seen for loss of IGF2BP1.

FUBP3, also named MARTA2 has been reported to bind to the 3'-UTR of the localized MAP2 mRNA in rat neurons (42) and regulates its dendritic targeting (49). Although the binding site of FUBP3 in MAP2

mRNA is not known, its preferred binding motif (UAUA) was recently identified (57). This motif is present in the 3'-UTR of β-actin 405 bp downstream of the zipcode. FUBP proteins might play a more substantial role in RNA localization since homologs of a second member of the FUBP family, FUBP2 were not only reported to be involved in MAP2 or β-actin mRNA localization (49, 67) but also present among the biotinylated proteins we identified. However, FUBP2 is mainly nuclear and its role in β-actin mRNA localization might be indirect (67). In contrast, FUBP3 seems to have a direct function in localizing β-actin as it binds to the 3'-UTR and its loss reduces β-actin mRNA localization. We show that FUBP3 and IGF2BP1 do not bind directly to each other and IGF2BP1 levels are not affected by Fubp3 knockdown, ruling out an indirect effect on β-actin mRNA localization via changing IGF2BP1 amounts. What might therefore be the function of FUBP3? A potential function could be translational regulation. Like Igf2bp1 knockdown, loss of FUBP3 results in increased amounts of β-actin protein while β-actin mRNA levels are similar or even lower than in untreated MEFs. This could be due to a loss of translational inhibition as it has been shown for IGF2BP1.

Its role in β-actin and MAP2 mRNA localization suggests that FUBP3/MARTA2 is a component of several localizing mRNPs. Of note, RNA-BioID on β-actin mRNA has identified even more RBPs that have been previously involved in the localization of other mRNAs, e.g. SYNCRIP (68) or Staufen (46). Several of these like STAU1 and STAU2 are highly enriched in our β-actin biotinylated proteome. This finding might on one hand reflect the participation of multiple RBPs in β-actin localization or regulation. It also shows that a common set of RBPs is used to control the fate of several different localized mRNAs in different cell types. Although RNA-BioID does not currently allow us to determine if all these RBPs are constituents of the same β-actin mRNP, belong to different states of an mRNP or to different populations, their identification allows addressing these questions to reach a more detailed understanding of the common function of RBPs on diverse mRNAs.

Materials and methods

RNA-BioID: For RNA-BioID, cells were incubated with 50 µM biotin for 24 hrs. Following incubation, cells were washed twice with 1x PBS and lysed in IP lysis buffer (50 mM Tris pH 7.5, 150 mM NaCl, 2.5 mM $MgCl_2$, 1 mM DTT, 1% tween-20, and 1x protease inhibitor) and passed 10-12 times through a 21G needle. The lysate was cleared by centrifugation (12,000 x g for 10 min at 4°C) to remove cell debris. 10 µg of protein from the supernatant ('total cell lysate') were used to check for protein biotinylation. In the remaining lysate, NaCl was added to a final concentration of 500 mM. 200 µl of a streptavidin magnetic bead suspension (GE Healthcare) were added and the high salt lysate incubated overnight at 4°C with end to end rotation. On the next day, the beads were collected (by keeping the beads on the magnetic stand for 2 min) and washed as described before (69). In detail, they were washed twice for 5 min with 0.3 ml wash buffer 1 (2% SDS), once with wash buffer 2 (0.1% (w/v) deoxycholate, 1% (w/v) tween-20, 350 mM NaCl, 1 mM EDTA pH 8.0), once with wash buffer 3 (0.5% (w/v) deoxycholate 0.5% (w/v) tween-20, 1 mM EDTA, 250 mM LiCl, 10 mM Tris-HCl pH 7.4) and 50 mM Tris-HCl pH 7.5, once with wash buffer 4 (50 mM NaCl and 50 mM Tris-HCl pH 7.4), and finally twice with 500 µl of 50 mM ammonium bicarbonate. 20 µl of the beads were used for western blot and silver staining, and 180 µl was subjected to mass spectrometry analysis. To release captured proteins for western blot analysis from streptavidin beads, the beads were incubated in 2x Laemmli buffer containing 2 mM saturated biotin and 20 mM DTT for 10 min at 95 degree.

For biotinylation after serum induction, cells were starved for 24 hrs as described in material methods and induced with 10% serum containing media containing 50 µM biotin for at least for 6 hrs to 24 hrs. Samples were processed for mass spectrometric analysis as described in the material method section.

Plasmids and cloning: The lentivirus vector pHAGE-UbiC carrying NLS-2X MCP-tagRFPT (70) was used as backbone to generate all lentiviral vectors used in this study. In order to generate pHAGE-NLS-2XMCP-GFP, the GFP fragment was amplified from pEGFPC1 and cloned into the lentiviral vector within XbaI and ClaI restriction sites, thereby replacing the tagRFPT sequence. To generate pHAGE-NLS-2XMCP-eGFP-BirA*, a BirA* fragment was amplified from plasmid pSF3-TGN38-cMyc-BirA* (71) with XhoI and ClaI sites, eGFP fragment was amplified with XbaI and XhoI sites, after digestion both the fragments were ligated and the ligated product was PCR amplified using forward XbaI eGFP primer

and reverse ClaI BirA* primer and the amplified product was integrated into pHAGE-NLS-2XMCP-eGFP plasmid under XbaI and ClaI sites.

Plasmids expressing mCherry fusion proteins were generated on pcDNA3.1(+) backbone. The mCherry CDS was amplified from plasmid pmCherry-C1 (Clontech), introducing NotI and XhoI sites at the 5' or 3' ends and the PCR product ligated into pcDNA3.1(+) to generate a C-terminal tag mCherry pcDNA3.1(+) entry plasmid. To create a N-terminal tag mCherry pcDNA3.1(+) entry plasmid, mCherry was amplified with NheI-mCherry forward and AflIII-mCherry reverse primer and cloned at the beginning of the MCS of pcDNA3.1(+).

Coding sequences of Igf2bp1 (Acc.No. NM_009951.4) and Fubp3 (Acc.No. NM_001290548.1) were amplified from Mouse (C57BL/6J) cDNA and cloned into C-terminal mCherry using restriction sites NheI and EcoRI (for Igf2bp1), KpnI and NotI (Fubp3).

To create plasmids expressing KH mutants of Fubp3-mCherry, Fubp3-mCherry was chosen as the template and different primer sets (Supplementary table 2) were used for inverse PCR to change the G-X-X-G motifs to G-D-D-G (58). After treating the PCR reaction with DpnI for overnight at 37°C, the linear amplification product was transformed into *E.coli Dh5α* for re-ligation and amplification.

To create a backbone vector for *in vitro* transcription, plasmid pcDNA3.1 was modified (mod-pcDNA3.1(+)) to remove unwanted restriction sites and to introduce a new restriction site before the T7 promoter. Two primers were designed for inverse PCR of pcDNA3.1(+), resulting in an additional ClaI site in front of the T7 promoter while at the same time removing a part of the multiple cloning site. DNA sequences encoding the β-actin zipcode, the proximal zipcode or a mutant zipcode were generated by annealing two complimentary oligos containing NheI-ClaI overhangs at the ends and after phosphorylation ligated into the mod-pcDNA3.1(+) vector within NheI and ClaI sites. To generate pcDNA3.1(+) β-actin-3'UTR, the complete β-actin 3'UTR was amplified and cloned into the same sites.

Cell culture and serum starvation assay: Mouse embryonic fibroblasts (MEFs) from C57BL/6J mice or Hek293T cells were cultured in DMEM (with 4.5 g glucose and L-glutamine containing 10% fetal bovine serum (FBS) and 1% pen-strep). For serum starvation of MEFs, cells were starved in DMEM medium without serum (including 1% pen-strep) for at least 24 hrs and induced with DMEM media containing 10% FBS and 1% pen- strep for 1hr.

Lentivirus generation: Lentiviral particles were produced by transfecting the expression vector along with plasmids (Addgene plasmid numbers 12259, 12251, and 12253) for ENV (pMD2.VSVG), packaging (pMDLg/pRRE), and REV (pRSV-Rev) into HEK293T cells using Fugene HD reagent (Promega). The virus-containing supernatant was harvested on day 2 and day 3 and centrifuged at 500 x g for 10 min at 4˚ C and passed through 0.45 µm filter. The filtered supernatant was used for transduction of MEFs cells at a dilution of 1:100 and in presence of 8 mg/ml protamine sulfate. 3 days after the transfection, MEFs were washed 3x with serum containing media, trypsinized and washed twice again. Cells were washed once in FACS buffer (1x DPBS without calcium and magnesium, 0.2% BSA, 0.5 mM EDTA, 5 mM $MgCl_2$) and resuspended in FACS Cells expressing low levels of GFP were isolated with a FACS Aria cell sorter (Becton-Dickinson) before further culturing.

Immunoprecipitation, Western blot, and qRT-PCR: For immunoprecipitation (IP), cells were lysed in IP lysis buffer (35). At least 200 µg of total protein was used per pull down experiment. For the rest of the experiment including western and qPCR, the protocol was followed as mentioned before (72) with the following modifications. A total of 200 µg of proteins were taken after lysing the cells in IP lysis buffer. 100 µl of protein A (for anti-mouse antibodies) or protein G (for anti-rabbit antibodies) coupled magnetic beads were used for IP. After washing them 3x in NT2 buffer (72) the beads were blocked with 5% BSA and 0.5 mg/ml ssDNA. After washing the beads once again with NT2 buffer, the beads were incubated with either 20 µg of FUBP3 antibody (Abcam) or 10 µl of IGF2BP1 anti-mouse antibody (Clone 6A957) (73) in NT2 buffer at a total volume of 200µl, for overnight at 4°C with end to end rotation. After preclearing the lysates with 100µl of protein A or Protein G mag beads, antibody coupled beads were added in the lysates and incubated for 4 hrs at 4°C with end to end rotation. After the incubation, beads were separated from the lysates by a magnetic stand and washed 5 times with ice cold NT2 buffer and the supernatant was removed. Beads were resuspended in 100 µl of NT2 buffer. For isolation of proteins from the beads, 40 µl of beads were boiled in 100 µl 1x Laemmli buffer for 10 min at 95 C and the elute was separated from the beads on a magnetic strand. For western blots 40 µl from the eluted sample were used. For RNA isolation, in the 60 µl of the remaining beads, 5 µl proteinase K (10 mg/ml) and 1 µl of 10% SDS were added and incubated at 55°C water bath for 30 min. 100 µl of buffer NT2 was added in the sample and 200 µl of acidic phenol-chloroform mix was added and vortexed for 10 sec. After centrifugation at 16,000g at room temperature for 5 min, the upper aqueous layer was

isolated, sodium acetate (pH 5.2, final concentration 0.3 M), 5 µl glycoblue (Invitrogen), and 600 µl of ethanol was added to precipitate the RNA. The RNA pellet was resuspended in 50 µl of RNase free water. For qPCR analysis, 500 ng of RNA was used after treating with 10U of DNase I.

Igf2bp1 and Fubp3 knockdown: For knockdown experiments, cells were treated with Accell SMARTpool siRNAs (Dharmacon) at a concentration of 1µM for 72-96 hrs and the protocol was followed as suggested by the manufacturer. The SMARTpool of siRNAs used against Igf2bp1 were 5'-CUCCAAAGUUCGAAUGGUC-3', 5'-CUUUUAAACGUGGAUUGUC-3', 5'-UUGUUAAGAUCAUCGGACA-3', 5'-CUUCUUGGUUAAUUCACGA-3', for Fubp3, 5'-GAACUAUUAUGUAUUGUAA-3', 5'-GUGUGAGGAUCCAAUUCAA-3', 5'-CUGUGAAACACUAUAUUUA-3', 5'-UUAUGAUGCUUGAAAUGUC-3'. As a control the Accell Mouse Control siRNA Kit was used.

NanoLC-MS/MS analysis and data processing: Beads were resuspended in denaturation buffer (6 M urea, 2 M thiourea, 10 mM Tris buffer, pH 8.0), and proteins were reduced by incubation in 1 mM dithiothreitol (DTT) for 1 h at room temperature. Alkylation of reduced cysteines was performed in 5.5 mM iodoacetamide (IAA) in 50 mM ammonium bicarbonate (ABC) buffer for 1 h at room temperature in the dark. On beads digestion of proteins was started with endoproteinase LysC (2 µg per 100 µg protein) for 3 h of incubation at pH 8.0 and room temperature. Tryptic digestion (2 µg per 100 µg protein) was performed overnight at room temperature after diluting the sample with four volumes of 20 mM ABC and adjusting the pH to 8.0. Acidified peptides were purified via PHOENIX Peptide Clean-up Kit (PreOmics) according to user manual, and separated on an EasyLC nano-HPLC (Thermo Scientific) coupled to an LTQ Orbitrap Elite (Thermo Scientific) as described elsewhere (74) with slight modifications: The peptide mixtures were injected onto the column in HPLC solvent A (0.1% formic acid) at a flow rate of 500 nl/min and subsequently eluted with an 87 minutes segmented gradient of 5–33-50-90% of HPLC solvent B (80% acetonitrile in 0.1% formic acid) at a flow rate of 200 nl/min. Precursor ions were acquired in the mass range from m/z 300 to 2000 in the Orbitrap mass analyzer at a resolution of 120,000. Accumulation target value of 106 charges was set. The 15 most intense ions were sequentially isolated and fragmented in the linear ion trap using collision-induced dissociation (CID) at the ion accumulation target value of 5000 and default CID settings. Sequenced precursor

masses were excluded from further selection for 60 s. Acquired MS spectra were processed with MaxQuant software package version 1.5.2.861 with integrated Andromeda search engine (75). Database search was performed against a target-decoy *Mus musculus* database obtained from Uniprot, containing 60,752 protein entries, the sequence of MCP-eGFP-BirA and 284 commonly observed contaminants. Endoprotease trypsin was defined as protease with a maximum of two missed cleavages. Oxidation of methionine and N-terminal acetylation were specified as variable modifications, whereas carbamidomethylation on cysteine was set as fixed modification. Initial maximum allowed mass tolerance was set to 4.5 ppm (for the survey scan) and 0.5 Da for CID fragment ions. Peptide, protein and modification site identifications were reported at a false discovery rate (FDR) of 0.01, estimated by the target/decoy approach (76). The label-free algorithm was enabled, as was the "match between runs" option (77).

Downstream analysis and functional interpretation: Downstream analyses were performed in the R environment (78). The resultant proteome profiles obtained were quality checked for replicate correlation using principal component analysis and hierarchical clustering. The data was then filtered for low abundant proteins via a two-step process. Firstly, all proteins were ranked (in descending order) by LFQ intensity and the 3rd quartile LFQ value set as the minimum intensity threshold. Secondly, to pass the filtering, all samples within a condition must have an LFQ intensity above this threshold. Contaminants and reverse hits, as well as proteins only identified by sites, were also removed from downstream analyses. Following low abundance filtering the LFQ values were quantile normalized using the MSnbase package (79). In order to statistically compare protein abundances across conditions (even when the protein was not detected in one of the conditions) imputation was used on the data using a mixed model of nearest neighbour averaging and left-censored missing data from a truncated distribution (79). Comparisons in which both conditions contained imputed values were completely discounted. Proteins which were significantly different between conditions were identified using ANOVA followed by the Tukey post-hoc test. Significance was set at an adjusted p-value of 0.05 following Benjamini-Hochberg multiple correction testing. Functional information, namely gene ontology (GO) and KEGG ID, for *Mus musculus* proteins were retrieved using the UniProt.ws package (80). The over-representation testing for GO and KEGG pathways were done for each comparison via the cluster

Profiler package67 based on hypergeometric distribution (p-adj. ≤ 0.05). Further analysis were performed using the Perseus software (80, 81).

Expression of recombinant proteins and in vitro binding assay with *in vitro* transcribed RNA: Full length Igf2bp1, Fubp3, were cloned into pGEX6p-1 plasmid containing a GST tag. For Fubp3-pGEX6p-1 1704bp long Fubp3 was cloned into SmaI and NotI site after GST tag and 1724bp long Igf2bp1 was cloned under BamHI site after the GST tag. The proteins were expressed in Rossetta-gami™ 2(DE3) cells according to manufacturer's protocol (Novagen). 683 bp long full length β-actin 3'UTR, the 54 nt long localization element of β-actin, the 49 bp long region proximal to the zipcode, or mutated zipcode (82) were cloned between NheI and ClaI site into a modified pCDNA3.1(+) as mentioned before (Cloning part), that contains a T7 promoter but lacks the CMV promoter. For in vitro transcription the plasmids were linearized with NheI. and 1µg of the linearized purified plasmids were used, 10 µl of 40 mM Tris-HCl, pH 7.5, 6 mM MgAc2, 10 mM DTT, 1 mM spermidine, 0.5 mM each of ATP, GTP and CTP, 10 µM UTP. 100 units/ml RNase inhibitor and 500 units/ml of T7 RNA polymerase, for 1 h at 37°C. RNA was recovered by ethanol precipitation at -20°.

For the *in vitro* binding assay, 100 µg of total protein lysates were pre-cleared with empty magnetic beads before incubation with 50 pmol of in vitro transcribed RNAs at 4°C for at least 4 hrs with end to end rotation. GST tagged proteins and bound RNAs were captured with anti GST Mag beads (GE), washed twice with 1xPBS, once with buffer containing 250 mM NaCl and 10 mM Tris-HCl pH7.5 and finally once with 10 mM Tris-HCl pH7.5. Half of the beads were used for protein isolation and western blot. And the rest was used for RNA isolation. RNA amounts were determined after reverse transcription, by qRT PCR (primer list).

Immunofluorescence and smFISH: WT MEFs or MEFs containing MS2 tagged β-actin but not MCP-GFP were seeded on cover glass in a 6 well cell culture plate and grown for 24 hr in serum free media before serum containing media was added to the cells for 1-2 hrs. Cells were then washed three times with PBS, fixed for 10 min with 3.7% formaldehyde in PBS, washed three times in PBS and incubated for at least one hour in 70% ethanol at 4°C. Following that, cells were washed with wash buffer (10% formamide in 2XSSC) and incubated ON at 28°C in hybridization solution (10% w/v dextran sulfate, 2mM vanadyl-ribonucleuoside, 0.02% RNase free BSA,10% formamide, 2XSSC) containing 125ng

probes and primary antibody (FUBP3 1:50, IGF2BP1 1:400, VIGILIN 1:250). After incubation, cells were washed 3x for 5 min in wash buffer, before the secondary antibody (1:500 in hybridization solution) was applied for 60-90 min at room temperature. Cells were then washed twice for 30 min in wash buffer, incubated with 2XSSC for 2 - 5 min before mounting them on a microscope slide (Immu-mount, Thermo Scientific). Optionally 5 ng/ml bis-benzimide was added in the second wash for nuclear staining. In case of smFISH only, cells were incubated ON at 37°C with hybridization buffer containing just 10% dextran sulfate and 10% formamide in 2XSSC. Sequences of MBS probes and β-actin ORF probes are described in table S4. Primary antibody sources and working concentrations are detailed in table S3.

Microscopy and object-based colocalization analysis: Cells were imaged with a Zeiss Cell Observer wide field fluorescence microscope, operated by ZEN software (Zeiss), Illuminated with xenon arc lamp and detected with a CCD camera (Axiocam 506). For the colocalization experiments and the live cell imaging we used either 63x/1.4 plan apochromat or 100x/1.45 α-plan fluar oil immersion objectives (Zeiss). For the Knockdown experiments we used 40x/1.3 EC Plan neo fluar oil immersion objective (Zeiss). For the live cell imaging we used a dual band GFP/mCherry filter set (F56-319, AHF). For the smFISH-IF Images we used either the dual band GFP/mCherry filter or the combination of the 38-HE and F45 filter set from Zeiss. We imaged the cells using 240 nm z-axis step size over 2 microns. Representative slices were subjected to image processing and object-based localization. Particles were identified using the Mexican hat filter plug-in available for Fiji which apply Laplacian of Gaussian filter to a 2D image. Object based localization was performed using the xsColoc ImageJ plugin as described (50). Briefly, the plugin determines the colocalization of objects in single snapshot frames by measuring the distance between closest neighbour objects from the β-actin mRNP (reference channel) and the protein or other probes set (target channel). Particles from each channel were first detected using different parameters and the maximal distance allowed between two objects was set to 500 nm. A region of interest was selected (cell without the nucleus) and then the features of all the particles from the reference channel and the features of colocalizing particles, if found, from the target channel were identified. The identified particles from the reference channel are then randomly assigned to clusters in the size of 100 particles and the fraction of objects from the reference channel colocalizing with the target channel were then used for the second level of analysis where the mean and the SD of all the clusters is calculated and represented then as the observed colocalization.

Extraction, statistical analysis and plotting of the data produced by the xsColoc plugin were carried out in R using the R Studio front-end (https://www.rstudio.com/) and the ggplot2 library (69) to plot the graphs. The R script to analyse the data was written and kindly provided by Imre Gaspar.

Data availability: Proteomic data supporting this study has been deposited into PRIDE, accession no: PXD010694.

Author Contributions: JM and RPJ conceived the project. JM and OH performed experiments, analysed the data and wrote the manuscript. MFW, NN, JM, and BM designed, performed and analysed the mass spectrometry experiments. RPJ supervised the project, interpreted the data and wrote the manuscript.

Acknowledgement: We thank Jeff Chao (FMI, Basel), Imre Gaspar (EMBL, Heidelberg), Julién Bethune (BZH, Heidelberg), Stefan Kindler (U. Hamburg), Stefan Hüttelmaier (U. Halle), and Ibrahim Muhammad Syed (IFIB, U. Tübingen) for plasmids, cell lines, antibodies, or spike RNA. We are grateful to Frank Essmann (IFIB, U. Tübingen) and Silke Wahle (PCT, U. Tübingen), for technical support and Matthew Cheng (IFIB, U. Tübingen) for suggestions on the manuscript. The project was funded by the Deutsche Forschungsgemeinschaft (DFG-FOR2333).

REFERENCES:

1. Martin KC, Ephrussi A (2009) mRNA localization: gene expression in the spatial dimension. *Cell* 136(4):719–30.
2. Eliscovich C, Buxbaum AR, Katz ZB, Singer RH (2013) mRNA on the move: the road to its biological destiny. *J Biol Chem* 288(28):20361–8.
3. Marchand V, Gaspar I, Ephrussi A (2012) An Intracellular Transmission Control Protocol: Assembly and transport of ribonucleoprotein complexes. *Curr Opin Cell Biol*. 24(2):202-10.
4. Dreyfuss G, Kim VN, Kataoka N (2002) Messenger-rna-binding proteins and the messages they carry. *Nat Rev Mol Cell Biol* 3(3):195–205.
5. Kislauskis EH, Zhu X, Singer RH (1997) beta-Actin messenger RNA localization and protein synthesis augment cell motility. *J Cell Biol* 136(6):1263–70.

6. Condeelis J, Singer RH (2005) How and why does beta-actin mRNA target? *Biol Cell* 97(1):97–110.

7. Lawrence JB, Singer RH (1986) Intracellular localization of messenger RNAs for cytoskeletal proteins. *Cell* 45(3):407–15.

8. Ross AF, Oleynikov Y, Kislauskis EH, Taneja KL, Singer RH (1997) Characterization of a beta-actin mRNA zipcode-binding protein. *Mol Cell Biol* 17(4):2158–65.

9. Lionnet T, et al. (2011) A transgenic mouse for in vivo detection of endogenous labeled mRNA. *Nat Methods* 8(2):165–170.

10. Park HY, Trcek T, Wells AL, Chao JA, Singer RH (2012) An Unbiased Analysis Method to Quantify mRNA Localization Reveals Its Correlation with Cell Motility. *Cell Rep*. 1(2):179-84.

11. Katz ZB, et al. (2012) β-actin mRNA compartmentalization enhances focal adhesion stability and directs cell migration. *Genes Dev*. 26(17):1885-90.

12. Bassell GJ, et al. (1998) Sorting of beta-actin mRNA and protein to neurites and growth cones in culture. *J Neurosci* 18(1):251–265.

13. Yao J, Sasaki Y, Wen Z, Bassell GJ, Zheng JQ (2006) An essential role for beta-actin mRNA localization and translation in Ca2+-dependent growth cone guidance. *Nat Neurosci* 9(10):1265–1273.

14. Fernandez-Moya SM, Bauer KE, Kiebler MA (2014) Meet the players: local translation at the synapse. *Front Mol Neurosci*. 7: 84.

15. Kislauskis EH, Zhu X, Singer RH (1994) Sequences responsible for intracellular localization of beta-actin messenger RNA also affect cell phenotype. *J Cell Biol* 127(2):441–51.

16. Chao JA, et al. (2010) ZBP1 recognition of beta-actin zipcode induces RNA looping. *Genes Dev* 24(2):148–58.

17. Yisraeli JK (2005) VICKZ proteins: a multi-talented family of regulatory RNA-binding proteins. *Biol Cell* 97(1):87–96.

18. Yoon YJ, et al. (2016) Glutamate-induced RNA localization and translation in neurons. *Proc Natl Acad Sci U S A* 113(44):E6877–E6886.

19. Hüttelmaier S, et al. (2005) Spatial regulation of β-actin translation by Src-dependent phosphorylation of ZBP1. *Nature* 438(7067):512–515.

20. Wächter K, Köhn M, Stöhr N, Hüttelmaier S (2013) Subcellular localization and RNP formation

of IGF2BPs (IGF2 mRNA-binding proteins) is modulated by distinct RNA-binding domains. *Biol Chem* 394(8):1077–1090.

21. Ceci M, et al. (2012) RACK1 is a ribosome scaffold protein for β-actin mRNA/ZBP1 complex. *PLoS One* 7(4): e35034.
22. Pan F, Huttelmaier S, Singer RH, Gu W (2007) ZBP2 Facilitates Binding of ZBP1 to β-Actin mRNA during Transcription. *Mol Cell Biol* 27(23):8340–8351.
23. Itoh M, Haga I, Li Q-H, Fujisawa J (2002) Identification of cellular mRNA targets for RNA-binding protein Sam68. *Nucleic Acids Res* 30(24):5452–64.
24. Klein ME, Younts TJ, Castillo PE, Jordan BA (2013) RNA-binding protein Sam68 controls synapse number and local β-actin mRNA metabolism in dendrites. *Proc Natl Acad Sci* 110(8):3125–3130.
25. Rackham O, Brown CM (2004) Visualization of RNA-protein interactions in living cells: FMRP and IMP1 interact on mRNAs. *EMBO J*. 23(16):3346-55.
26. Dormoy-Raclet V, et al. (2007) The RNA-Binding Protein HuR Promotes Cell Migration and Cell Invasion by Stabilizing the β-actin mRNA in a U-Rich-Element-Dependent Manner. *Mol Cell Biol* 27(15):5365–5380.
27. Lee FCY, Ule J (2018) Advances in CLIP Technologies for Studies of Protein-RNA Interactions. *Mol Cell*. 69(3):354-369.
28. Hafner M, et al. (2010) Transcriptome-wide identification of RNA-binding protein and microRNA target sites by PAR-CLIP. *Cell* 141(1):129–41.
29. Castello A, et al. (2012) Insights into RNA biology from an atlas of mammalian mRNA-binding proteins. *Cell* 149(6):1393–406.
30. Zielinski J, et al. (2006) In vivo identification of ribonucleoprotein-RNA interactions. *Proc Natl Acad Sci* 103(5):1557–1562.
31. Rogell B, et al. (2017) Specific RNP capture with antisense LNA/DNA mixmers. *RNA* 23(8):1290–1302.
32. Gaspar I, Wippich F, Ephrussi A (2017) Enzymatic production of single-molecule FISH and RNA capture probes. *RNA* 23(10):1582–1591.
33. Slobodin B, Gerst JE (2010) A novel mRNA affinity purification technique for the identification of interacting proteins and transcripts in ribonucleoprotein complexes. *RNA* 16(11):2277–2290.

34. Roux KJ, Kim DI, Burke B (2013) BioID: A screen for protein-protein interactions. *Curr Protoc Protein Sci* 74:Unit 19.23.

35. Kim DI, et al. (2014) Probing nuclear pore complex architecture with proximity-dependent biotinylation. *Proc Natl Acad Sci* 111(24):E2453–E2461.

36. Gupta GD, et al. (2015) A Dynamic Protein Interaction Landscape of the Human Centrosome-Cilium Interface. *Cell* 163(6):1484–1499.

37. Roux KJ, Kim DI, Raida M, Burke B (2012) A promiscuous biotin ligase fusion protein identifies proximal and interacting proteins in mammalian cells. *J Cell Biol*. 196 (6): 801.

38. Ramanathan M, et al. (2018) RNA–protein interaction detection in living cells. *Nat Methods*. 07–212 (2018).

39. Chung H-J, et al. (2006) FBPs Are Calibrated Molecular Tools To Adjust Gene Expression. *Mol Cell Biol* 26(17):6584–6597.

40. Quinn LM (2017) FUBP/KH domain proteins in transcription: Back to the future. *Transcription* 8(3):185–192.

41. Blichenberg a, et al. (1999) Identification of a cis-acting dendritic targeting element in MAP2 mRNAs. *J Neurosci* 19(20):8818–8829.

42. Rehbein M, Kindler S, Horke S, Richter D (2000) Two trans-acting rat-brain proteins, MARTA1 and MARTA2, interact specifically with the dendritic targeting element in MAP2 mRNAs. *Mol Brain Res* 79(1–2):192–201.

43. Peabody DS (1993) The RNA binding site of bacteriophage MS2 coat protein. *Embo J* 12(2):595–600.

44. Lawrence JB, Singer RH (1986) Intracellular localization of messenger RNAs for cytoskeletal proteins. *Cell*. 45(3):407-15.

45. Tyagi S, Alsmadi O (2004) Imaging native β-actin mRNA in motile fibroblasts. *Biophys J* 87(6):4153–4162.

46. Heraud-Farlow JE, Kiebler MA (2014) The multifunctional Staufen proteins: conserved roles from neurogenesis to synaptic plasticity. *Trends Neurosci* 37(9):470–9.

47. Eliscovich C, Shenoy SM, Singer RH (2017) Imaging mRNA and protein interactions within neurons. *Proc Natl Acad Sci*. 114(10):E1875-E1884.

48. McDermott SM, Meignin C, Rappsilber J, Davis I (2012) Drosophila Syncrip binds the gurken

mRNA localisation signal and regulates localised transcripts during axis specification. *Biol Open* 1(5):488–497.

49. Zivraj KH, et al. (2013) The RNA-binding protein MARTA2 regulates dendritic targeting of MAP2 mRNAs in rat neurons. *J Neurochem* 124(5):670–684.
50. Gáspár I, Sysoev V, Komissarov A, Ephrussi A (2017) An RNA-binding atypical tropomyosin recruits kinesin-1 dynamically to oskar mRNPs. *EMBO J* 36(3):319–333.
51. Batish M, van den Bogaard P, Kramer FR, Tyagi S (2012) Neuronal mRNAs travel singly into dendrites. *Proc Natl Acad Sci U S A* 109(12):4645–50.
52. Designed Research; Y.-Y PPC, Pnas | S (2012) One influenza virus particle packages eight unique viral RNAs as shown by FISH analysis. 109(23):9101–9106.
53. Jønson L, et al. (2007) Molecular composition of IMP1 ribonucleoprotein granules. *Mol Cell Proteomics* 6(5):798–811.
54. Mingle LA, et al. (2005) Localization of all seven messenger RNAs for the actin-polymerization nucleator Arp2/3 complex in the protrusions of fibroblasts. *J Cell Sci* 118(11):2425–2433.
55. Kim HH, Lee SJ, Gardiner AS, Perrone-Bizzozero NI, Yoo S (2015) Different motif requirements for the localization zipcode element of β-actin mRNA binding by HuD and ZBP1. *Nucleic Acids Res* 43(15).43(15): 7432–7446.
56. Farina KL, Hüttelmaier S, Musunuru K, Darnell R, Singer RH (2003) Two ZBP1 KH domains facilitate β-actin mRNA localization, granule formation, and cytoskeletal attachment. *J Cell Biol* 160(1):77–87.
57. Dominguez D, et al. (2018) Sequence, Structure, and Context Preferences of Human RNA Binding Proteins. *Mol Cell* 70(5):854–867.e9.
58. Hollingworth D, et al. (2012) KH domains with impaired nucleic acid binding as a tool for functional analysis. *Nucleic Acids Res* 40(14):6873–86.
59. Stöhr N, et al. (2012) IGF2BP1 promotes cell migration by regulating MK5 and PTEN signaling. *Genes Dev* 26(2):176–89.
60. Schopp IM, et al. (2017) Split-BioID a conditional proteomics approach to monitor the composition of spatiotemporally defined protein complexes. *Nat Commun* 8:15690.
61. Rhee H-W, et al. (2013) Proteomic Mapping of Mitochondria in Living Cells via Spatially Restricted Enzymatic Tagging. *Science (80-)* 339(6125):1328–1331.

62. Fallini C, et al. (2014) Dynamics of survival of motor neuron (SMN) protein interaction with the mRNA-binding protein IMP1 facilitates its trafficking into motor neuron axons. *Dev Neurobiol* 74(3):319–332.

63. Donlin-Asp PG, et al. (2017) The Survival of Motor Neuron Protein Acts as a Molecular Chaperone for mRNP Assembly. *Cell Rep* 18(7):1660–1673.

64. Latham VM, Yu EH, Tullio AN, Adelstein RS, Singer RH (2001) A Rho-dependent signaling pathway operating through myosin localizes beta-actin mRNA in fibroblasts. *Curr Biol* 11(13):1010–6.

65. Song T, et al. (2015) Specific interaction of KIF11 with ZBP1 regulates the transport of β-actin mRNA and cell motility. *J Cell Sci* 128(5).128: 1001-1010.

66. Park HY, et al. (2014) Visualization of dynamics of single endogenous mRNA labeled in live mouse. *Science (80-)* 343(6169):422–424.

67. Gu W, Pan F, Zhang H, Bassell GJ, Singer RH (2002) A predominantly nuclear protein affecting cytoplasmic localization of β-actin mRNA in fibroblasts and neurons. *J Cell Biol* 156(1):41–51.

68. Donnelly CJ, Fainzilber M, Twiss JL (2010) Subcellular Communication Through RNA Transport and Localized Protein Synthesis. *Traffic*. 1498-505

69. Wickham H (2009) *Ggplot2* doi:10.1007/978-0-387-98141-3.

70. Halstead JM, et al. (2015) An RNA biosensor for imaging the first round of translation from single cells to living animals. *Science (80-)* 347(6228):1367–1370.

71. Béthune J, Artus-Revel CG, Filipowicz W (2012) Kinetic analysis reveals successive steps leading to miRNA-mediated silencing in mammalian cells. *EMBO Rep* 13(8):716–723.

72. Keene JD, Komisarow JM, Friedersdorf MB (2006) RIP-Chip: The isolation and identification of mRNAs, microRNAs and protein components of ribonucleoprotein complexes from cell extracts. *Nat Protoc* 1(1):302–307.

73. Bell JL, et al. (2013) Insulin-like growth factor 2 mRNA-binding proteins (IGF2BPs): Post-transcriptional drivers of cancer progression? *Cell Mol Life Sci* 70(15):2657–2675.

74. Franz-Wachtel M, et al. (2012) Global Detection of Protein Kinase D-dependent Phosphorylation Events in Nocodazole-treated Human Cells. *Mol Cell Proteomics* 11(5):160–170.

75. Cox J, et al. (2011) Andromeda: A peptide search engine integrated into the MaxQuant environment. *J Proteome Res* 10(4):1794–1805.

76. Elias JE, Gygi SP (2007) Target-decoy search strategy for increased confidence in large-scale protein identifications by mass spectrometry. *Nat Methods* 4(3):207–214.

77. Luber CA, et al. (2010) Quantitative Proteomics Reveals Subset-Specific Viral Recognition in Dendritic Cells. *Immunity* 32(2):279–289.

78. R Foundation for Statistical Computing (2016) R: A Language and Environment for Statistical Computing. *R Foundation for Statistical Computing* doi:10.1007/978-3-540-74686-7.

79. Gatto L, Lilley KS (2012) Msnbase-an R/Bioconductor package for isobaric tagged mass spectrometry data visualization, processing and quantitation. *Bioinformatics* 28(2):288–289.

80. Carlson M (2018) *UniProt.ws: A package for retrieving data from the UniProt web service* Available at: https://www.bioconductor.org/packages/devel/bioc/vignettes/UniProt.ws/inst/doc/UniProt.ws.pdf [Accessed August 2, 2018].

81. Tyanova S, et al. (2016) The Perseus computational platform for comprehensive analysis of (prote)omics data. *Nat Methods* 13(9):731–740.

82. Nicastro G, et al. (2017) Mechanism of β-actin mRNA Recognition by ZBP1. *Cell Rep* 18(5):1187–1199.

FIGURES:

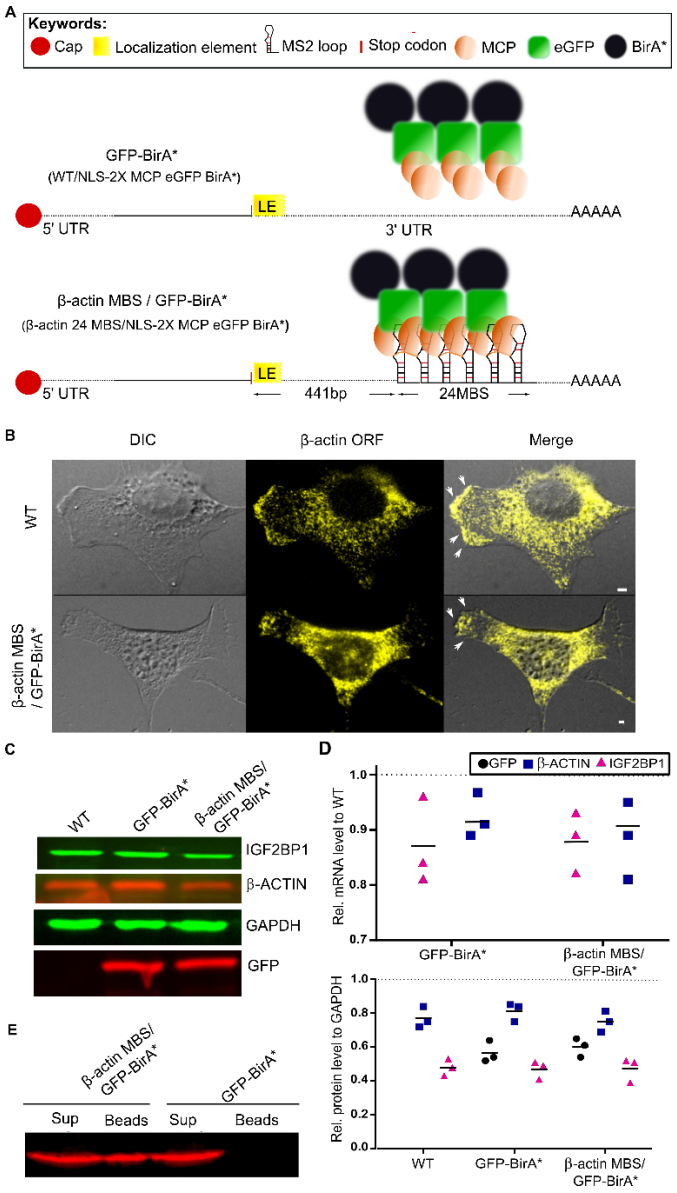

Fig 1: RNA BioID to detect proteins interacting with localized β-actin RNA.

(A) Schematic of the β-actin-MBS/GFP-BirA* (bottom: used to detect β-actin mRNA associated proteins) and control constructs, GFP-BirA* (top: used to detect background biotinylation due to overexpression of NLS-MCP-GFP-BirA*) constructs.

The 24xMS2 loop (24MBS) array was integrated in the 3'UTR of the endogenous β-actin gene 441 bp downstream of the stop codon. BirA* is targeted to 24MBS by fusing it to NLS-2xMCP-eGFP (bottom panel). Control cells express NLS-2xMCP-eGFP-BirA* and β-actin mRNA lacking the MBS cassette (top panel).

(B) Representative smFISH images of WT (top panel) and cells used to detect the β-actin mRNA associated proteins (as described in bottom panel in A) showing the proper localization of β-actin mRNA to the cell protrusions. β-actin mRNA was detected by probes against the β-actin ORF (yellow). scale bar: 5 µm

(C) Western blot images used for quantification in (D).

(D) Top: Quantification of β-actin and Igf2bp1 mRNA levels and MEFs expressing β-actin-MBS and MCP-GFP-BirA* or only MCP-GFP-BirA*. Data are derived from 3 biological replicas and normalized to expression levels of corresponding mRNAs in wildtype MEFs. Line represents the median. Bottom: Protein levels of endogenous β-ACTIN, IGF2BP1, and heterologous MCP-GFP-BirA* (detected by anti-GFP antibody) are comparable in wildtype MEFs and MEFs expressing GFP-BirA*. Western blot signals were normalized to GAPDH. Data are derived from 3 biological replicas. Line represents the median.

(E) Biotinylation of IGF2BP1 depends on MBS sites in β-actin. Following RNase A treatment, biotinylated proteins were affinity-purified with streptavidin-coated beads from cells expressing 2xMCP-eGFP-BirA* in the presence (β-actin-24MBS) or absence (β-actin) of MCP binding sites (MBS). Presence of IGF2BP1 was probed by a specific antibody in bead fraction (Beads) and supernatant (Sup).

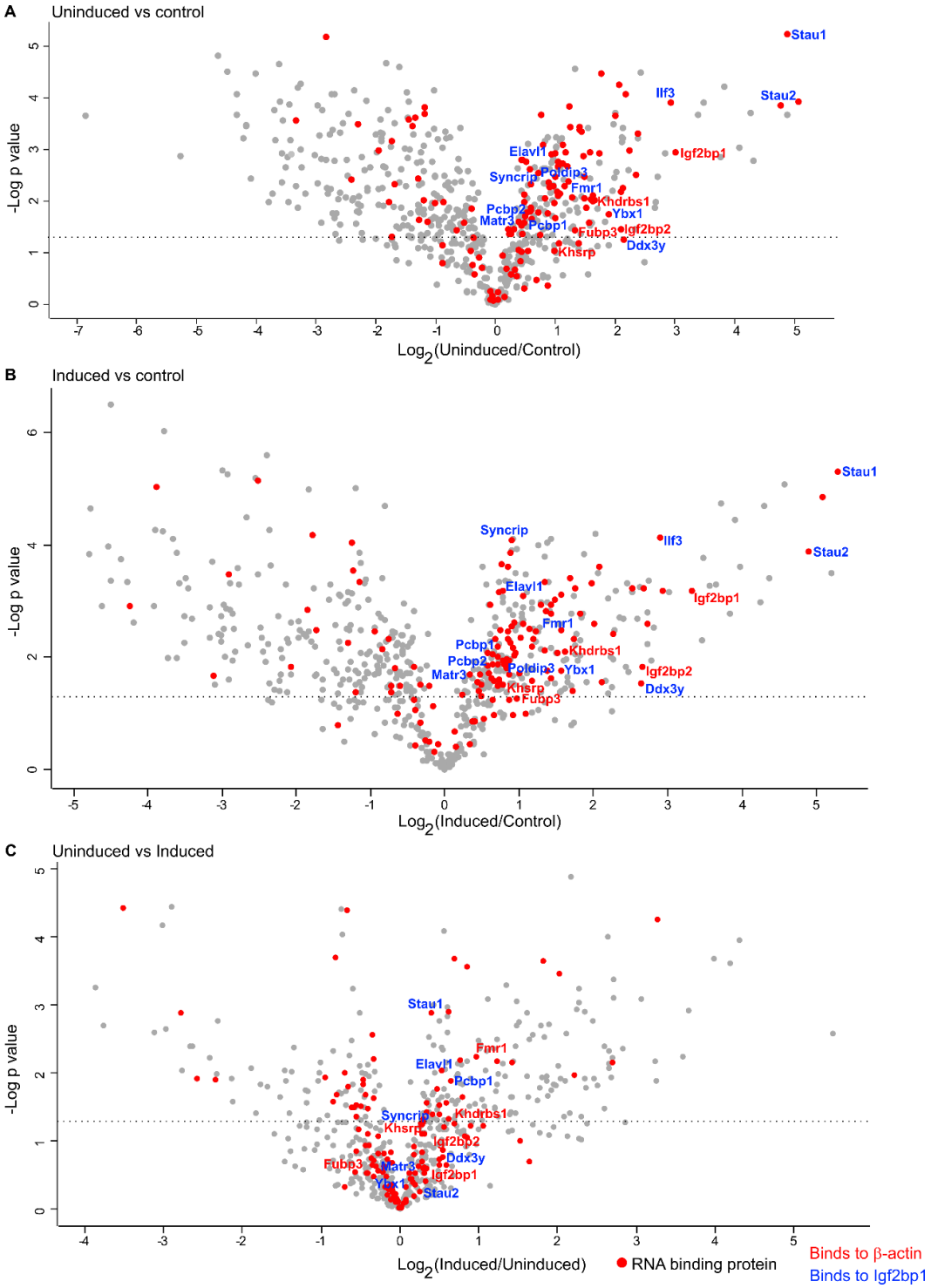

Fig 2: Enrichment of biotinylated proteins in control MEFs, or MEFs expressing β actin-MBS-BirA* under serum-induced or uninduced conditions.

Volcano plot representation of biotinylated proteins in
(A) uninduced MEFs compared to control MEFs,
(B) serum-induced MEFs compared to control MEFs.
(C) serum-induced MEFs compared to uninduced MEFs.
In the volcano plots, the X-axis represents log2 fold change in protein abundance and the Y-axis represents the –log10 p-value. Red circles are known RBPs identified by GO-molecular function analysis. Proteins names in red represent known β-actin mRNA interactors and proteins named in blue are RBPs known to bind to IGF2BP1. Dotted line indicates p = 0.05.

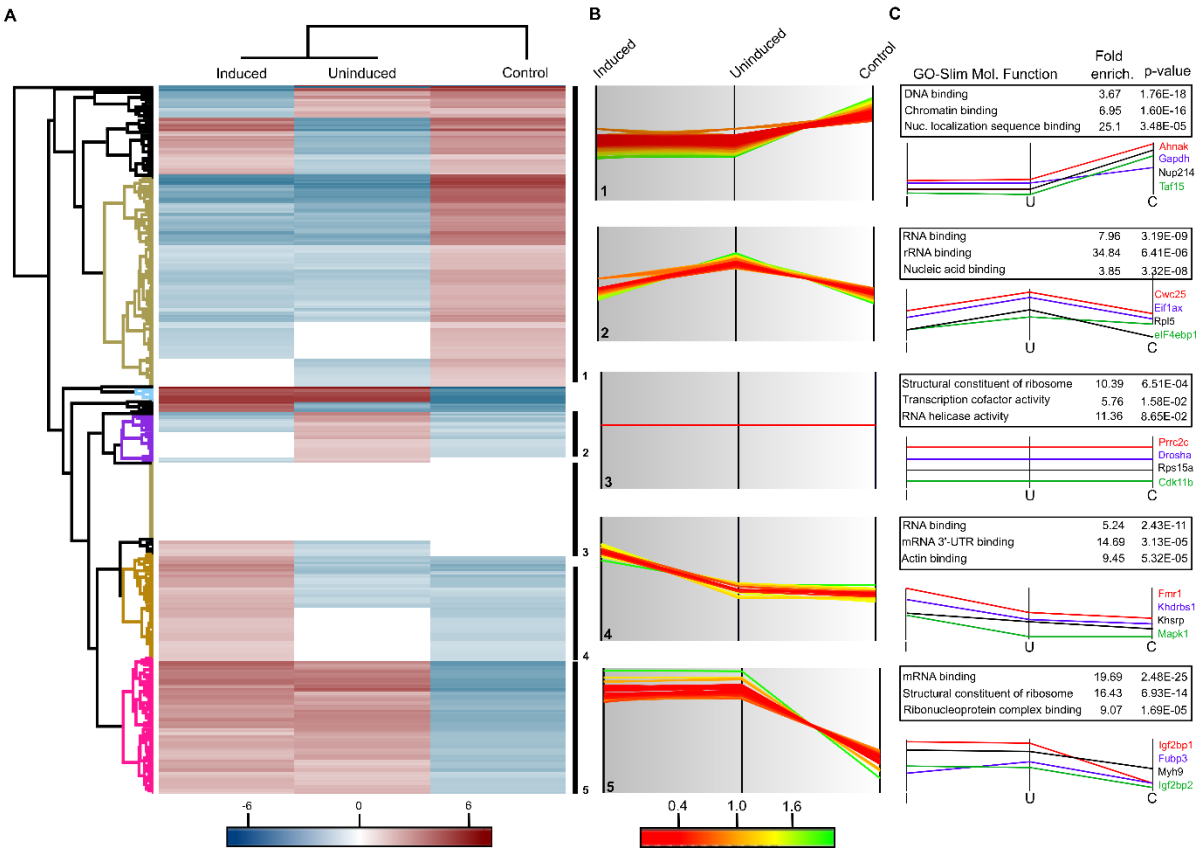

Fig 3: Cluster analysis of biotinylated proteins in control MEFs or MEFs expressing β-actin-MBS-BirA* under serum-induced or uninduced conditions.

(A) Hierarchical clustering of biotinylated proteins in serum-induced, uninduced β-actin-MBS-BirA* MEFs and control MEFs (lacking β-actin-MBS). Enrichment is indicated in red colouring, depletion in blue. Various clusters of protein groups are highlighted in the dendrogram.

(B) Profile plots of five selected clusters showing distinct enrichment patterns of biotinylated proteins: 1. Strongly enriched in control MEFs; 2. Enriched in β-actin-MBS-BirA* MEFs under uninduced condition; 3. Similar enrichment in all MEFs. 4. Enriched in β-actin-MBS-BirA* MEFs under serum-induced conditions; 5. Enriched in β-actin-MBS-BirA* MEFs under serum induced and uninduced conditions compared to the control MEFs. Degree of enrichment in each specific cluster is represented by colouring (green, more enriched, red, less enriched).

(C) Functional analysis of protein annotation terms results in multiple categories that are enriched in the selected clusters. GO-slim molecular function terms, the corresponding enrichment factor, and the p-value are shown in the table. Selected examples of proteins found in each cluster are depicted below the tables.

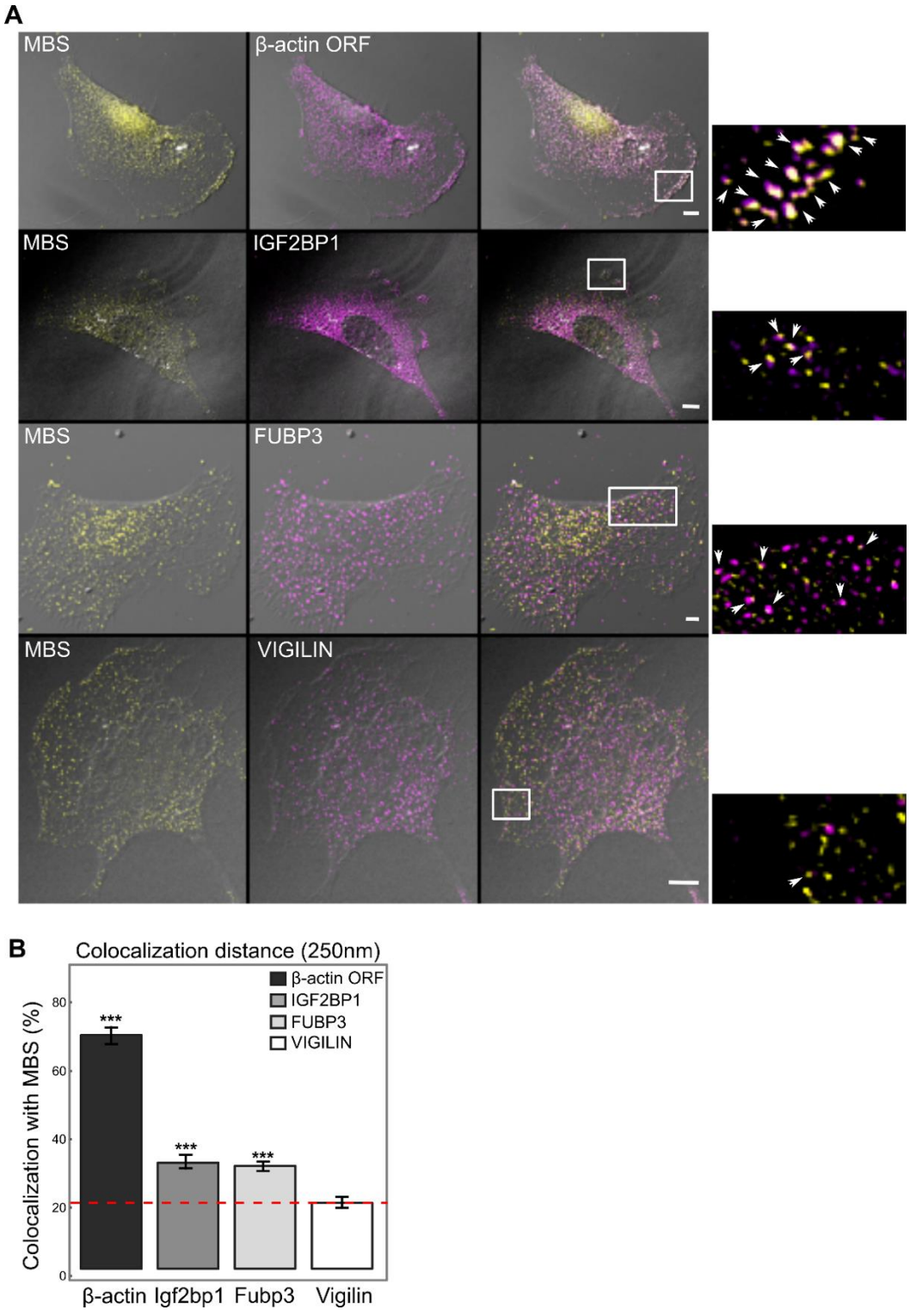

Fig 4: Colocalization of IGF2BP1 and FUBP3 with β-actin-MBS mRNA.
(A) Representative smFISH-immunofluorescence images in MEFs expressing β-actin-MBS. RNA is detected with smFISH probes against MBS (yellow) or against β-actin ORF (magenta), proteins with antibodies against either IGF2BP1, FUBP3 or VIGILIN (magenta). Boxed areas indicate magnified regions from images taken with at least 63x magnification. Arrows indicate colocalizing objects. Scale bar represent 5 μm.
(B) Degree of colocalization of β-actin-MBS with β-actin ORF, IGF2BP1, FUBP3 or VIGILIN. Histogram bars represent the ratio of colocalization at the maximal colocalization distance of 250 nm. The red dotted line indicates background colocalization as defined by colocalization of the MBS site with the control RBP VIGILIN. Error bars represent 95% confidence interval. Unpaired t test *** P<0.001.

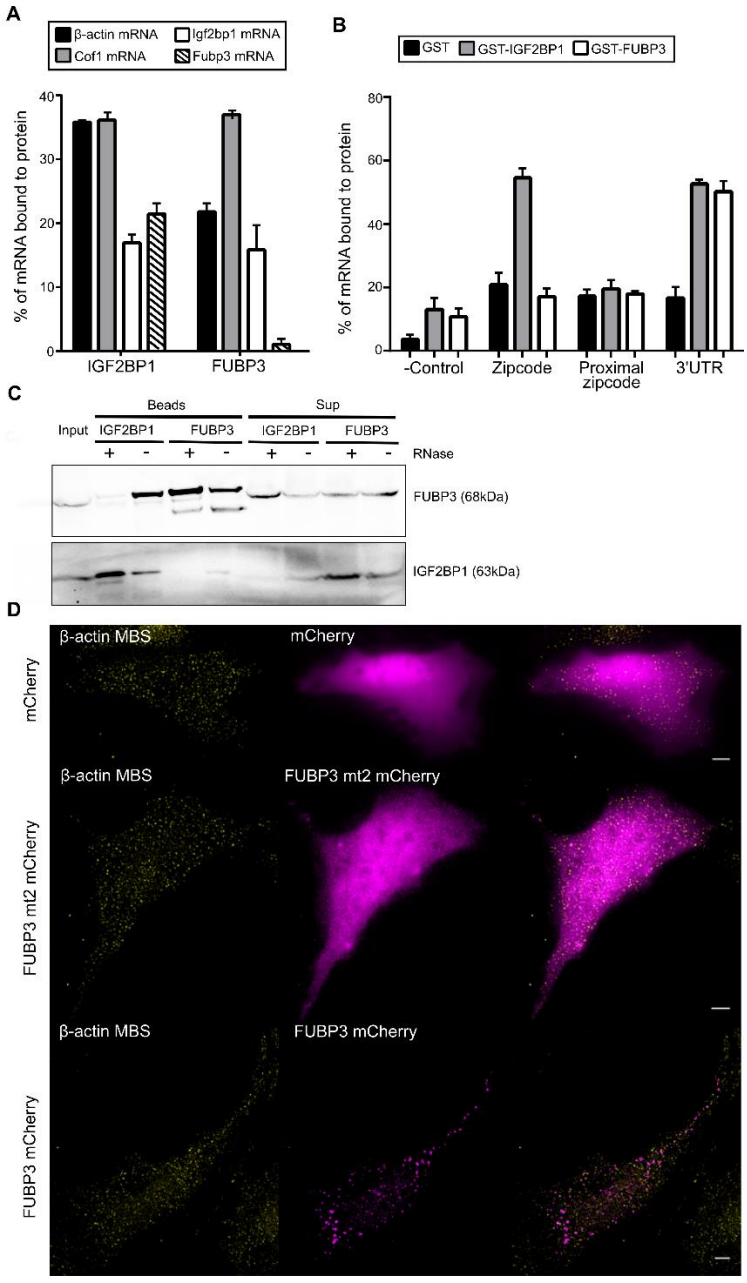

Fig 5: FUBP3 binds to β-actin 3'UTR.

(A) Co-immunoprecipitation of selected mRNAs with IGF2BP1 and FUBP3. Bars represent percentage of input mRNA co-purifying with the indicated protein. IGF2BP1 binds to several endogenous mRNAs such as Cofilin1, Igf2bp1, and Fubp3. FUBP3 binds to 23% of endogenous β-actin mRNA while IGF2BP1 was associated with 37% of endogenous β-actin mRNA. Error bars represents mean ± sem from three independent experiments.

(B) RNA pulldown of GST fusion proteins of IGF2BP1 and FUBP3. *In vitro* transcribed RNA fragments of β-actin (zipcode, proximal zipcode, full-length 3'UTR, and a zipcode mutant as negative control) were added to *E. coli* lysates with expressed GST or GST fusion proteins. Fusion proteins and bound RNAs were affinity-purified and bound RNA detected by quantitative RT-PCR. Bars represent percentage of input RNA. In contrast to IGF2BP1, FUBP3 shows little affinity for the zipcode sequence but binds to the 3'UTR. Error bars represents mean±sem from three independent experiments.

(C) Co-immunoprecipitation of FUBP3 and IGF2BP1. Immunoprecipitation was performed from wild type MEFs either with anti-FUBP3 or -IGF2BP1 antibodies in presence and absence of RNase A. IGF2BP1 only co-precipitates with FUBP3 in absence of RNase A.

(D) RNA-binding domain KH2 is required for FUBP3 cytoplasmic granule formation. The conserved G-X-X-G motif of FUBP3 KH domains were individually mutated into G-D-D-G and wildtype and mutant proteins expressed in MEFs as mCherry fusion. Live cell imaging shows that wild type FUBP3-mCherry forms cytoplasmic granules whereas a KH2 mutant (FUBP3 mt2) is evenly distributed in the cytoplasm like the control mCherry protein. Scale bar represent 5 μm.

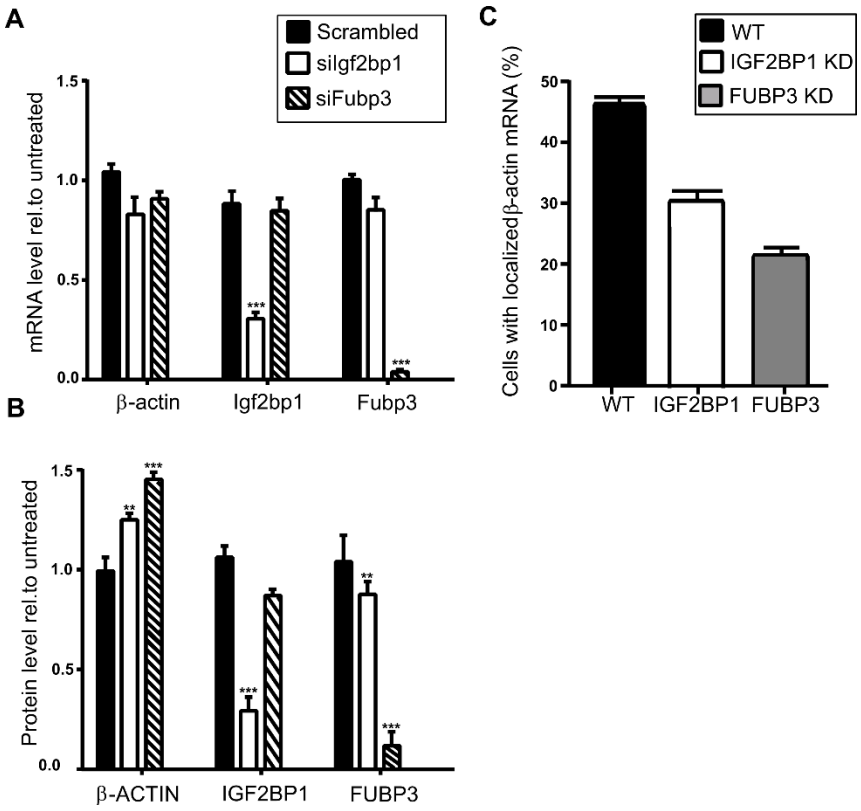

Fig 6: Downregulation of Fubp3 affects β-actin mRNA localization.
(A)-(C) Cells were treated for 72 hrs with scrambled siRNAs or siRNAs against Fubp3 or Igf2bp1.
(A) Quantitative RT-PCR analysis of Igf2bp1, β-actin, Fubp3 levels in knockdown cells. mRNA levels in untreated cells were used for normalization.
(B) Western blot analysis of IGF2BP1, β-ACTIN, FUBP3 protein levels in knockdown cells. Protein levels in untreated cells were used as normalization control.
(C) Percentage of cells with localized β-actin mRNA in wild type MEFs and upon depletion of Igf2bp1 or Fubp3. Total number of cells analysed is 562 in wild type, 241 in Igf2bp1 knockdown MEFs and 343 in Fubp3 knockdown MEFs. Localization of β-actin-MBS mRNA to the cell protrusions was manually scored by smFISH against β-actin MBS.
Statistical significance of each dataset was determined by Student's t-test; **P < 0.01; ***P < 0.001. Error bars represents mean±sem from 3 independent experiments.